




## Quantum transport in flat bands and supermetallicity

G. Bouzerar \*

CNRS, Université Claude Bernard Lyon 1, F-69622 Lyon, France

D. Mayou 

Université Grenoble Alpes, CNRS, Institut NEEL, F-38042 Grenoble, France

 (Received 24 June 2020; revised 30 October 2020; accepted 21 January 2021; published 9 February 2021)

Quantum physics in flat-band (FB) systems embodies a variety of exotic phenomenon and even counterintuitive features. The quantum transport in several graphene based compounds that exhibit a flat band and a tunable gap is investigated. Despite the localized nature of the FB states and a zero group velocity, a supermetallic (SM) phase at the FB energy is revealed. The SM phase is robust against the inelastic scattering strength and controlled only by the interband transitions between the FB and the dispersive bands. The SM phase appears insensitive and quasi-independent of the gap amplitude and nature of the lattice (disordered or nanopatterned). The universal nature of the unconventional FB transport is illustrated with the case of electrons in the Lieb lattice.

DOI: [10.1103/PhysRevB.103.075415](https://doi.org/10.1103/PhysRevB.103.075415)

Over the past decade, we have witnessed a growing interest for the physics in flat-band (FB) systems. In these systems, and because of destructive quantum interferences, the electron group velocity is exactly zero, and the kinetic energy is quenched. This gives rise to various exotic physical phenomena, such as topological states [1–3], superconductivity [4,5], Wigner crystal [6,7], and ferromagnetism [8–10]. The wealth and fascinating physics that take place in these systems motivate the search for efficient procedures and strategies for flat-band engineering. For instance, twisted bilayer graphene is known to feature isolated and relatively flat bands near charge neutrality, when tuned to special magic angles only [11–14]. Recently, it has been suggested that robust FB can be realized in van der Waals patterned dielectric superlattices that could be controlled by gate voltage [15]. Nanolithography, molecular engineering, and 3D printing are also possible pathways to design complex two-dimensional materials [16–19]. The field of cold atoms on artificial lattices also offers a platform to address these fundamental issues since it allows the direct tuning of the physical parameters of the model Hamiltonians [20–23].

The important progress made in the realization of complex and nanostructured materials has stimulated theoretical studies in fractalized systems [24–28]. Recently, considering the case of the graphene Sierpinski carpet where the fractalization induces (i) a  $E = 0$  flat band and (ii) a gap in the spectrum, we have reported an unusual form of quantum electronic transport [29]. Despite the gap, an unexpected supermetallic (SM) phase, insensitive to the strength of the inelastic scattering rate, appears at the neutrality point with a conductivity that coincides within a few percent with  $\sigma_0 = \frac{4e^2}{\pi h}$  that of the pristine compound. In this system, the transport is controlled by interband transitions only, between the FB and the valence (conduction) band.

Our goal is to address the crucial and inevitable question that naturally arises: Is this unusual form of quantum electronic transport universal? More precisely, does the SM flat-band transport take place in other types of systems? For that purpose, we consider three different situations that lead to a FB at  $E = 0$  and a gap in the spectrum: (i) the fully uncompensated graphene (FUG) where vacancies are randomly distributed on the same sublattice and two self-similar lattices, (ii) the Sierpinski carpet (GSC), and (iii) the Sierpinski gasket (GSG). The choice for graphene is also motivated by the fact that it has emerged as an outstanding system for fundamental research [30–33]. Note that the GSC conductivity as studied in detail in Ref. [29] will be used just for comparison with the gasket case. Transport is expected to be drastically different in the gasket than in the carpet. The Sierpinski carpet is infinitely ramified while the gasket only finitely. In other words, the gasket can be deconstructed by removing a finite number of sites while it requires an infinite one for the carpet [34].

To address the second question, we consider the electronic transport in the Lieb lattice (the  $\text{CuO}_2$  planes in cuprates) where the spectrum is gapless and a FB meets the conduction band and the valence band at the Dirac point. It is nowadays possible to realize experimentally the Lieb lattice either by manipulating cold atoms in optical lattices [35–37] or by direct laser writing of optical waveguides [38–40], and it could even be synthesized by means of covalent organic frameworks [41].

Electrons in the FB systems, as illustrated in Fig. 1, are modeled by a nearest-neighbor tight-binding Hamiltonian that reads

$$\hat{H} = -t \sum_{\langle ij \rangle, s} c_{is}^\dagger c_{js} + \text{H.c.}, \quad (1)$$

where  $\langle ij \rangle$  denotes nearest neighbor pairs.  $c_{is}^\dagger$  creates an electron with spin  $s$  at site  $\mathbf{R}_i$ . In the Lieb lattice the only allowed hoppings are between the nearest neighbor pairs  $(A, B)$  and  $(A, C)$ .

\*georges.bouzerar@univ-lyon1.fr

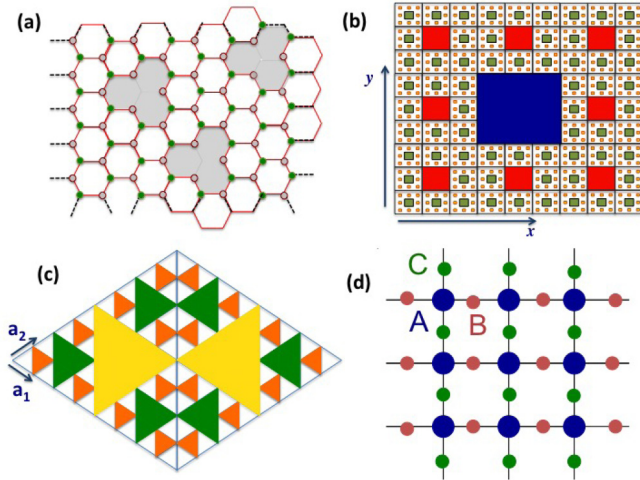


FIG. 1. Illustration of (a) the fully uncompensated graphene (FUG), (b),(c) the graphene Sierpinski carpet (GSC) and gasket (GSG), and (d) the Lieb lattice. In (a), (b), and (c) the colored area corresponds to the regions of removed atoms.

The GSC is constructed from a square piece of graphene of length  $L = 3^{i_c+1}a$  ( $a$  is the nearest neighbor C-C distance). We use for the GSC's the notation  $(i_c, f)$  where  $f$  is the degree of “fractalization” that varies from 0 (pristine) to its maximum value  $f_{\max} = i_c$ . The GSG is obtained from a triangular piece of graphene delimited by the vectors  $N\mathbf{a}_1$  and  $N\mathbf{a}_2$  where  $\mathbf{a}_1$  and  $\mathbf{a}_2$  are the unit cell vectors of graphene and  $N = 2^{i_g+1}$ . It is then symmetrized with respect to the  $y$  axis to give a diamond piece of graphene. Because of the symmetrization, the GSG contains the same number of C atoms on both sublattices. The GSG is specified by the notation  $(i_g, f)$ . Here, our study is restricted to optimally fractalized compounds only:  $f = i_c$  for the carpet and  $f = i_g$  for the gasket. The lattice geometry is unimportant for the FUG case. Periodic boundary conditions along  $x$  and  $y$  directions (see Fig. 1) are used for the FUG, the GSC, and the Lieb lattice and along  $\mathbf{a}_1$  and  $\mathbf{a}_2$  for the GSG.

The conductivity along the  $x$  direction is given by the Kubo-Greenwood formula [42,43],

$$\sigma(E) = \frac{e^2 \hbar}{\pi \Omega} \text{Tr}[\text{Im} \hat{G}(E) \hat{v}_x \text{Im} \hat{G}(E) \hat{v}_x]. \quad (2)$$

The current operator is defined by  $\hat{v}_x = -\frac{i}{\hbar} [\hat{x}, \hat{H}]$  and the Green's function  $\hat{G}(E) = (E + i\eta - \hat{H})^{-1}$ .  $\Omega$  is the sample area and  $\eta$  mimics an energy independent inelastic scattering rate with a characteristic timescale  $\tau_{in} = \frac{\hbar}{\eta}$ . For the FUG, the GSG, and the GSC the calculations are done using the Chebyshev polynomial Green's function method (CPGF) [44–46] that (i) allows large scale calculations as it requires a modest amount of memory and (ii) a CPU cost that varies only linearly with the system size  $N_S$ . CPGF has proven to be a powerful tool to address the nature of the magnetic couplings in disordered materials [47,48]. In the same spirit as CPGF, the conductivity could be also calculated by quantum wave packet dynamics as well [49–51]. The FUG, the GSC, and the GSG considered contain approximately  $3.5 \times 10^6$  sites. The number of random vectors  $N_R$  used for the stochastic trace calculation is 50. The number of Chebyshev polynomials kept

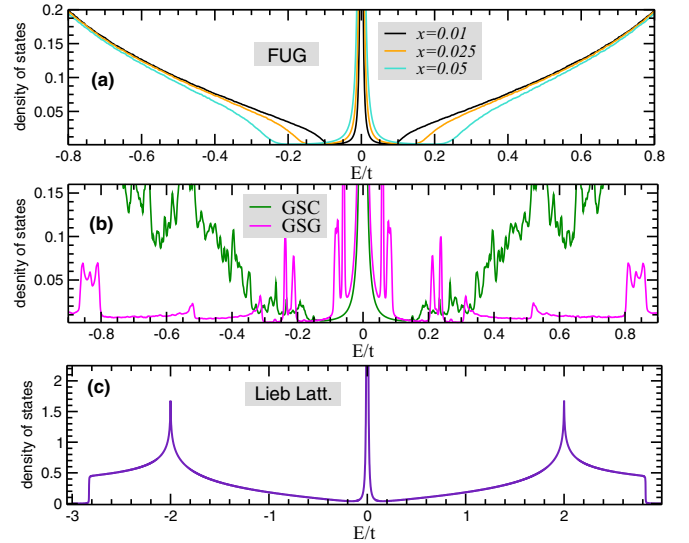


FIG. 2. Density of states (in  $1/t$ ) in (a) the FUG for three different concentrations of vacancies,  $x = 0.01, 0.025,$  and  $0.05$ , (b) in the GSG and in the GSC, and (c) in the Lieb lattice. The systems used for the calculations are  $(7,7)$  for the GSC, and  $(11,11)$  for the GSG (see the notations in the text). The FUG contains approximately  $3.5 \times 10^6$  sites.

is  $M = 2500$ , leading to a  $M \times M$  matrix of moments used for the conductivity calculation. It has been checked that both  $N_R$  and  $M$  were sufficient to reach convergence. On the other hand, the calculations are realized analytically in the case of the Lieb lattice.

Figure 2 depicts the electronic density of states (DOS)  $\rho(E) = -\frac{1}{\pi N_S} \text{Tr}[\text{Im} \hat{G}(E)]$  as a function of the energy in the graphene compounds and in the Lieb lattice. As expected for the FUG, a  $\delta$  peak at  $E = 0$  appears and a gap which increases with the density of randomly distributed A vacancies [52]. The gap ( $\Delta$ ) from the valence (resp. conduction) band to the FB of zero energy modes (ZEM) is  $0.10t, 0.15t,$  and  $0.20t$  for, respectively,  $x = 0.01, 0.025,$  and  $0.05$ . The DOS has a richer texture in the fractal lattices. Besides a gap,  $\Delta = 0.135t$  in the GSC and significantly larger in the GSG where it is approximately  $0.31t$ , we observe complex fluctuating substructures that result from the fractal nature of the eigenspectrum. In the GSG, we observe many extended low-DOS regions interspersed by sharp peaks. This reflects a one-dimensional-like characteristic that originates from the finitely ramified fractal lattice. In the GSG, in addition to a central ZEM peak, several pronounced satellite peaks appear at  $E = \pm 0.06t, \pm 0.077t, \pm 0.085t, \pm 0.22t,$  and  $\pm 0.24t$ , revealing additional, almost flat bands. The exact diagonalization calculations on smaller systems,  $(4,4), (5,5),$  and  $(6,6)$ , have confirmed that these subbands are not rigorously flat, in contrast to the  $E = 0$  band. In addition, in both the FUG and the GSC the number of ZEM states ( $N_{\text{ZEM}}$ ) is exactly  $|N_A - N_B|$ ,  $N_A$  (resp.  $N_B$ ) being the number of C atoms on sublattice A (resp. B), as it is expected in bipartite lattices [52,53]. In the GSC, the ZEM density,  $x_{\text{ZEM}}$ , is approximately 0.05. In contrast, the situation is different in the GSG, where by construction  $N_A = N_B$  (see Fig. 1). The expected  $x_{\text{ZEM}}$  should be zero, which is not the case. It varies with the system

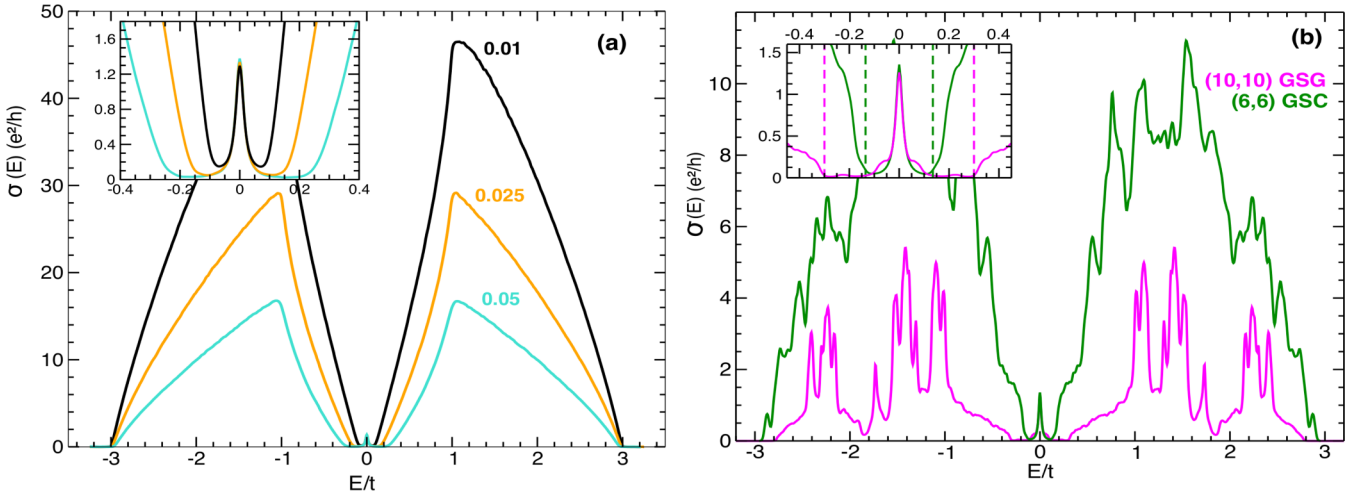


FIG. 3. Conductivity (in  $\frac{e^2}{h}$ ) at  $T = 0$  K as a function of the energy in (a) the FUG and (b) the GSC and GSG. In (a) we consider three different concentrations of vacancies  $x = 0.01, 0.025,$  and  $0.05$ ; the systems contain approximately  $3.5 \times 10^6$  sites. In (b) the GSC and the GSG are, respectively, (6, 6) and (10, 10) systems.  $\sigma(0)$  is  $1.26\frac{e^2}{h}$  in the GSG and  $1.365\frac{e^2}{h}$  in the GSC. Here  $\eta = 0.016t$  but  $\sigma(0)$  is found insensitive to  $\eta$ . The insets magnify the neutrality point region.

size and we find  $x_{ZEM} = 0.164, 0.172, 0.177,$  and  $0.178$  in the (8,8), (9,9), (10,10), and (11,11), respectively, indicating a convergence towards 0.18. If  $N_A^L$  (resp.  $N_B^L$ ) is the number of  $A$  (resp.  $B$ ) sites of the ‘left’ triangle of the GSG diamond,  $|N_A^L - N_B^L|$  is also different from  $N_{ZEM}$ . Figure 2(c) illustrates the well known DOS in the Lieb lattice. It reveals three bands, two dispersive, which form a Dirac cone at the  $M$  point of the Brillouin zone and a FB at  $E = 0$ . We recall, in this case, that the local charge density of the localized,  $E = 0$  states, is nonzero on  $B$  and  $C$  sublattices only.

We discuss the electronic transport in these systems, with a focus on the central region. In the FUG, the conductivity  $\sigma(E)$  is depicted in Fig. 3(a) for different concentrations of vacancies. Besides a maximum in the valence band (VB) and conduction band (CB) at  $E = \pm t$  (Van Hove singularities in pristine graphene),  $\sigma(E)$  is finite for  $|E| \geq \Delta$  and decreases, as expected, as  $x$  increases. However, a close look at the FB vicinity reveals a peak that varies very weakly with  $x$ ,  $\sigma(0)$  coincides within a few percent with that of the pristine case,  $\sigma_0$ . We have also checked that  $\sigma(0)$  is insensitive to  $\eta$ , with  $\eta$  ranging from  $0.001t$  to  $0.05t$ . We should stress that our calculations correspond to the thermodynamic limit, as is illustrated in the Supplemental Material [54]. For  $|E| \leq \Delta$ ,  $\sigma(E)$  gets narrower and narrower as  $\eta$  decreases and can be nicely fitted by a Lorentzian of width  $\eta$ . However, our results disagree with those of Ref. [49] where  $\sigma(0) = 0$  is found. In this work,  $\sigma(E)$  is obtained from the Einstein formula and a direct calculation of the diffusivity from wave packet propagation. The singular DOS at  $E = 0$  and the fact that their calculations correspond to the limit  $\eta = 0$ , may explain the discrepancy.

Let us consider how self-similarity affects the electronic transport. Results, for a fixed  $\eta$ , are depicted in Fig. 3(b). The conductivity in the GSC has been discussed in details in Ref. [29]. It is only considered to facilitate the comparison with the gasket case and show the universality of the FB quantum transport. In the GSG,  $\sigma(E)$  is much smaller than that of the GSC and the peaks appear sharper. In the inset,

we observe a clear gap in the GSG of  $0.31t$  much larger than that of the GSC ( $0.135t$ ), as seen in the DOS (Fig. 2). A peak at  $E = 0$  is also clearly visible with values close to  $\sigma_0$ . More precisely, we find  $\sigma(0) = 1.07\sigma_0$  in the GSC and  $0.99\sigma_0$  in the GSG. Note also, for the GSG, shoulders that are absent for the GSC. They correspond to the states located at  $E = \pm 0.06t, \pm 0.077t,$  and  $\pm 0.085t$  in the DOS. We have checked that these shoulders disappear as  $\eta$  reduces (see Ref. [54]). Compared to the FB states, these satellite states behave in a more ‘‘standard’’ way. They are localized impurity states, leading to a vanishing conductivity when  $\eta \rightarrow 0$ . These results are robust, with negligible size effects (see Ref. [54]). Hence, from Fig. 3(a) and Fig. 3(b) we conclude that these graphene based systems lead to the same conclusion: a universal quantum transport at  $E = 0$  with a supermetallic flat band and a conductivity that reduces to the interband term (the intraband contribution vanishes). Remark that an important interband term was also at the origin of the quantum electronic transport anomalies in the icosahedral quasicrystals  $\alpha$ -AlMnSi [55]. The interband supermetallic regime can be visualized as a quantum transport controlled by the velocity fluctuations in systems where its average is very small or zero.

Finally, we address the possibility of FB induced SM phase in a very different system, the Lieb lattice. Figure 4(a) depicts  $\sigma(E)$  as a function of  $E$  for different values of  $\eta$ . As in the graphene based systems, a peak at  $E = 0$  is revealed [more visible in the inset of Fig. 4(b)]. However, in the Lieb lattice,  $\sigma(E = 0)$  increases slowly as  $\eta$  decreases ( $\eta$  varies by two orders of magnitude). The inset of Fig. 4(b) shows, for  $\eta/t = 10^{-2}$ , the decomposition in terms of the intraband ( $\sigma_{\text{intra}}$ ) and the interband ( $\sigma_{\text{inter}}$ ) contributions. The only nonvanishing matrix elements of the velocity operator that contribute to  $\sigma_{\text{inter}}$  are between the FB and the CB (resp. VB) states; those between VB and CB states are zero. We find that  $\sigma_{\text{intra}}$  is finite at  $E = 0$ . A focus on the  $\eta$  dependence of  $\sigma(0)$ , as is plotted in Fig. 4(b), shows that  $\sigma_{\text{intra}}(0)$  is constant and equals  $0.318\frac{e^2}{h}$ .

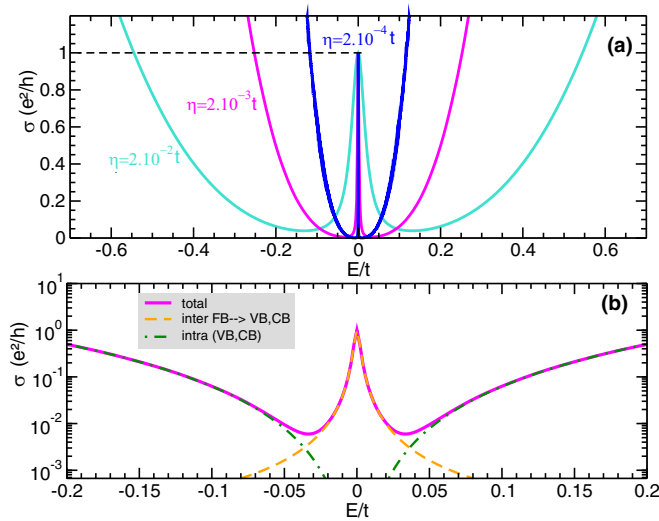


FIG. 4. (a) Conductivity in the Lieb lattice as a function of the energy  $E$  for different values of  $\eta$ . (b) Different contributions to  $\sigma(0)$  as a function of  $\ln(\eta/t)$ . (Inset)  $\sigma(E)$  (total, interband, and intraband) as a function of  $E$  for  $\eta = 2 \times 10^{-3} t$ .

On the other hand,  $\sigma_{\text{inter}}(0)$  has an unusual logarithmic dependence on  $\eta$ . We find, numerically,  $\sigma_{\text{inter}}(0) = \sigma_1 + \sigma_2 |\ln(\eta/t)|$  where  $\sigma_1 = 0.784 \frac{e^2}{h}$  and  $\sigma_2 = 0.637 \frac{e^2}{h}$ . Using the linear dispersion of the valence and conduction bands in the vicinity of the Dirac point, we find the following analytical expressions:  $\sigma_{\text{intra}}(0) = \frac{1}{\pi} \frac{e^2}{h}$ ,  $\sigma_2 = \frac{2}{\pi} \frac{e^2}{h}$ , and  $\sigma_1 = \frac{2}{\pi} \ln(E_c/t) \frac{e^2}{h}$  where  $E_c$  is the cutoff energy. Using a normalized DOS for the dispersive bands, we end up with  $\sigma_1 = 0.806 \frac{e^2}{h}$ .

We propose now to discuss the  $\eta$  dependence of the diffusivity in the SM phase. In the gapped cases, for both  $\eta$  and  $|E|$  smaller than  $\Delta$ ,  $\rho(E)$  reduces to  $\frac{N_{\text{ZEM}}}{\pi\Omega} \frac{\eta}{E^2 + \eta^2}$ . Equation (2) of the conductivity can be rewritten,

$$\sigma(E) = \left( \frac{4\hbar}{N_{\text{zem}}} \sum_{\alpha, \lambda = \pm, \beta} \frac{|\langle \Psi_\beta | \hat{v}_x | \Phi_\alpha^\lambda \rangle|^2}{E_\alpha^2} \eta \right) e^2 \rho(E), \quad (3)$$

where we have introduced  $|\Phi_\alpha^\lambda\rangle$ , the valence ( $\lambda = -$ ), and conduction ( $\lambda = +$ ) eigenstates with energy  $\pm|E_\alpha|$  and the FB eigenstates  $|\Psi_\beta\rangle$ . From the Einstein formula, the diffusivity  $D(E) = \frac{\sigma(E)}{e^2 \rho(E)}$  is straightforwardly obtained. It scales linearly with  $\eta$ , instead of the  $1/\eta$  behavior in standard metallic systems where  $D = \frac{1}{2} v_F^2 \frac{\hbar}{\eta}$ . In the gapless case of the Lieb lattice, the transport is still controlled by the interband term but the diffusivity has now two contributions,  $D = D_0 \eta + D_1 |\eta \cdot \ln(\eta)|$ . We expect, by introducing vacancies in the Lieb lattice, that a gap should open and the conductivity might lose the  $|\ln(\eta)|$  contribution and  $\sigma_{\text{intra}}(0)$  should vanish. All the features reported here justify the use of the term “supermetallicity” and generalize what has been found in the peculiar case of the GSC [29].

Notice that transport in the gapless dice lattice in the presence of random onsite potentials has revealed, in the weak disorder regime, a conductivity that varies logarithmically with the disorder strength [56]. Because, in the vicinity of  $E = 0$ , the electronic band structure is similar in the dice lattice and in the Lieb lattice, one expects the transport to behave similarly. Here, for vanishing  $\eta$ ,  $\sigma(0)$  diverges; this agrees with what has been found in the dice lattice in the limit of vanishing disorder.

In conclusion, in standard systems, the quantum transport is dictated by the average intraband velocity of the carriers; here at the FB energy, it is of interband nature. In all cases investigated, a SM phase, controlled by the off-diagonal matrix elements of the current operator, is revealed at the FB energy. In the graphene based systems, the conductivity is independent of the gap value, nature of the lattice, and inelastic scattering strength, and coincides within a few percent with  $\sigma_0$  ( $\frac{4e^2}{\pi h}$ ). In the gapless case of electrons, the Lieb lattice, the FB conductivity is found to vary logarithmically with the inelastic scattering strength ( $\sigma \approx \frac{1}{2} \sigma_0 |\ln(\eta)|$ ). This shows that the unconventional supermetallicity of the flat bands has a universal character. Based on the recent progress in the realization of complex 2D systems and in optical lattice physics, we hope that our findings will stimulate experimental studies.

- [1] E. Tang, J.-W. Mei, and X.-G. Wen, *Phys. Rev. Lett.* **106**, 236802 (2011).
- [2] K. Sun, Z. Gu, H. Katsura, and S. Das Sarma, *Phys. Rev. Lett.* **106**, 236803 (2011).
- [3] T. Neupert, L. Santos, C. Chamon, and C. Mudry, *Phys. Rev. Lett.* **106**, 236804 (2011).
- [4] S. Miyahara, S. Kusuta, and N. Furukawa, *Physica C* **460**, 1145 (2007).
- [5] Y. Cao, V. Fatemi, A. Demir, S. Fang, S. L. Tomarken, J. Y. Luo, J. D. Sanchez-Yamagishi, K. Watanabe, T. Taniguchi, E. Kaxiras, R. C. Ashoori, and P. Jarillo-Herrero, *Nature (London)* **556**, 43 (2018).
- [6] C. Wu, D. Bergman, L. Balents, and S. Das Sarma, *Phys. Rev. Lett.* **99**, 070401 (2007).
- [7] C. Wu and S. Das Sarma, *Phys. Rev. B* **77**, 235107 (2008).
- [8] H. Tasaki, *Phys. Rev. Lett.* **69**, 1608 (1992); *Prog. Theor. Phys.* **99**, 489 (1998).
- [9] A. Mielke, *Phys. Rev. Lett.* **82**, 4312 (1999).
- [10] K. Noda, A. Koga, N. Kawakami, and T. Pruschke, *Phys. Rev. A* **80**, 063622 (2009).
- [11] J. M. B. Lopes dos Santos, N. M. R. Peres, and A. H. Castro Neto, *Phys. Rev. Lett.* **99**, 256802 (2007).
- [12] E. Suarez Morell, J. D. Correa, P. Vargas, M. Pacheco, and Z. Barticevic, *Phys. Rev. B* **82**, 121407(R) (2010).
- [13] R. Bistritzer and A. H. MacDonald, *Proc. Natl. Acad. Sci. USA* **108**, 12233 (2011).
- [14] G. Trambly de Laissardiere, D. Mayou, and L. Magaud, *Phys. Rev. B* **86**, 125413 (2012).
- [15] L.-k. Shi, J. Ma and J. C. W. Song, *2D Mater.* **7**, 015028 (2020).
- [16] J. Fowlkes, R. Winkler, B. B. Lewis, M. G. Stanford, H. Plank, and P. D. Rack, *ACS Nano* **10**, 6163 (2016).

- [17] A. Vyatskikh, *Nat. Commun.* **9**, 593 (2018).
- [18] S. N. Kempkes, M. R. Slot, S. E. Freeney, S. J. M. Zevenhuizen, D. Vanmaekelbergh, I. Swart, and C. Morais Smith, *Nat. Phys.* **15**, 127 (2019).
- [19] E. J. W. Berenschot, H. V. Jansen, and N. R. Tas, *J. Micromech. Microeng.* **23**, 055024 (2013).
- [20] I. Belopolski, S.-Y. Xu, N. Koirala, C. Liu, G. Bian, V. N. Strocov, G. Chang, M. Neupane, N. Alidoust, D. Sanchez, H. Zheng, M. Brahlek, V. Rogalev, T. Kim, N. C. Plumb, C. Chen, F. Bertran, P. Le Fèvre, A. Taleb-Ibrahimi, M.-C. Asensio, M. Shi, H. Lin, M. Hoesch, S. Oh, and M. Z. Hasan, *Sci. Adv.* **3**, e1501692 (2017).
- [21] I. Bloch, J. Dalibard, and W. Zwerger, *Rev. Mod. Phys.* **80**, 885 (2008).
- [22] M. Lewenstein, A. Sanpera, V. Ahufinger, B. Damski, A. Sen (De), and U. Sen, *Adv. Phys.* **56**, 243 (2007).
- [23] N. R. Cooper, J. Dalibard, and I. B. Spielman, *Rev. Mod. Phys.* **91**, 015005 (2019).
- [24] E. van Veen, S. Yuan, M. I. Katsnelson, M. Polini, and M. Tomadin, *Phys. Rev. B* **93**, 115428 (2016).
- [25] E. van Veen, A. Tomadin, M. Polini, M. I. Katsnelson, and S. Yuan, *Phys. Rev. B* **96**, 235438 (2017).
- [26] M. Fremling, M. van Hooft, C. M. Smith, and L. Fritz, *Phys. Rev. Research* **2**, 013044 (2020).
- [27] T. Westerhout, E. van Veen, M. I. Katsnelson, and S. Yuan, *Phys. Rev. B* **97**, 205434 (2018).
- [28] M. Brzezinska, A. M. Cook, and T. Neupert, *Phys. Rev. B* **98**, 205116 (2018).
- [29] G. Bouzerar and D. Mayou, *Phys. Rev. Research* **2**, 033063 (2020).
- [30] S. Das Sarma, S. Adam, E. H. Hwang, and E. Rossi, *Rev. Mod. Phys.* **83**, 407 (2011).
- [31] A. H. Castro Neto, F. Guinea, N. M. R. Peres, K. S. Novoselov, and A. K. Geim, *Rev. Mod. Phys.* **81**, 109 (2009).
- [32] A. K. Geim and K. S. Novoselov, *Nat. Mater.* **6**, 183 (2007).
- [33] V. Fal'ko, A. Geim, S. Das Sarma, A. MacDonald, and P. Kim, *Solid State Commun.* **149**, 1039 (2009).
- [34] *Topology and Condensed Matter Physics*, edited by S. M. Bhattacharjee, M. Mj, and A. Bandyopadhyay (Springer, Singapore, 2017).
- [35] R. Shen, L. B. Shao, B. Wang, and D. Y. Xing, *Phys. Rev. B* **81**, 041410(R) (2010).
- [36] N. Goldman, D. F. Urban, and D. Bercioux, *Phys. Rev. A* **83**, 063601 (2011).
- [37] V. Apaja, M. Hyrkas, and M. Manninen, *Phys. Rev. A* **82**, 041402(R) (2010).
- [38] R. A. Vicencio, C. Cantillano, L. Morales-Inostroza, B. Real, C. Mejía-Cortés, S. Weimann, A. Szameit, and M. I. Molina, *Phys. Rev. Lett.* **114**, 245503 (2015).
- [39] D. Guzman-Silva, C. Mejia-Corteés, M. A. Bandres, M. C. Rechtsman, S. Weimann, S. Nolte, M. Segev, A. Szameit, and R. A. Vicencio, *New J. Phys.* **16**, 063061 (2014).
- [40] S. Mukherjee, A. Spracklen, D. Choudhury, N. Goldman, P. Öhberg, E. Andersson, and R. R. Thomson, *Phys. Rev. Lett.* **114**, 245504 (2015).
- [41] B. Cui, X. Zheng, J. Wang, D. Liu, S. Xie, and B. Huang, *Nat. Commun.* **11**, 66 (2020).
- [42] R. Kubo, *J. Phys. Soc. Jpn.* **12**, 570 (1957).
- [43] D. A. Greenwood, *Proc. Phys. Soc.* **71**, 585 (1958).
- [44] A. Ferreira and E. R. Mucciolo, *Phys. Rev. Lett.* **115**, 106601 (2015).
- [45] J. H. Garcia, L. Covaci, and T. G. Rappoport, *Phys. Rev. Lett.* **114**, 116602 (2015).
- [46] A. Weisse, G. Wellein, A. Alvermann, and H. Fehske, *Rev. Mod. Phys.* **78**, 275 (2006).
- [47] R. Bouzerar, D. May, U. Löw, D. Machon, P. Melinon, S. Zhou, and G. Bouzerar, *Phys. Rev. B* **94**, 094437 (2016).
- [48] H. Lee, E. R. Mucciolo, G. Bouzerar, and S. Kettemann, *Phys. Rev. B* **86**, 205427 (2012).
- [49] A. Cresti, F. Ortman, T. Louvet, D. Van Tuan, and S. Roche, *Phys. Rev. Lett.* **110**, 196601 (2013).
- [50] G. Trambly de Laissardiere and D. Mayou, *Phys. Rev. Lett.* **111**, 146601 (2013).
- [51] F. Triozon, J. Vidal, R. Mosseri, and D. Mayou, *Phys. Rev. B* **65**, 220202(R) (2002).
- [52] V. M. Pereira, J. M. B. Lopes dos Santos, and A. H. Castro Neto, *Phys. Rev. B* **77**, 115109 (2008).
- [53] E. H. Lieb, *Phys. Rev. Lett.* **62**, 1201 (1989).
- [54] See Supplemental Material at <http://link.aps.org/supplemental/10.1103/PhysRevB.103.075415> for the absence of size effects and the influence of the inelastic scattering strength in the vicinity of the neutrality point.
- [55] G. Trambly de Laissardiere, J.-P. Julien, and D. Mayou, *Phys. Rev. Lett.* **97**, 026601 (2006).
- [56] We thank the referee for bringing this reference to our attention: M. Vigh, L. Oroszlány, S. Vajna, P. San-Jose, G. Dávid, J. Cserti, and B. Dóra, *Phys. Rev. B* **88**, 161413(R) (2013).